Lab on a Chip

Devices and applications at the micro- and nanoscale

rsc.li/loc

Platelets

ROYAL SOCIETY
OF **CHEMISTRY**
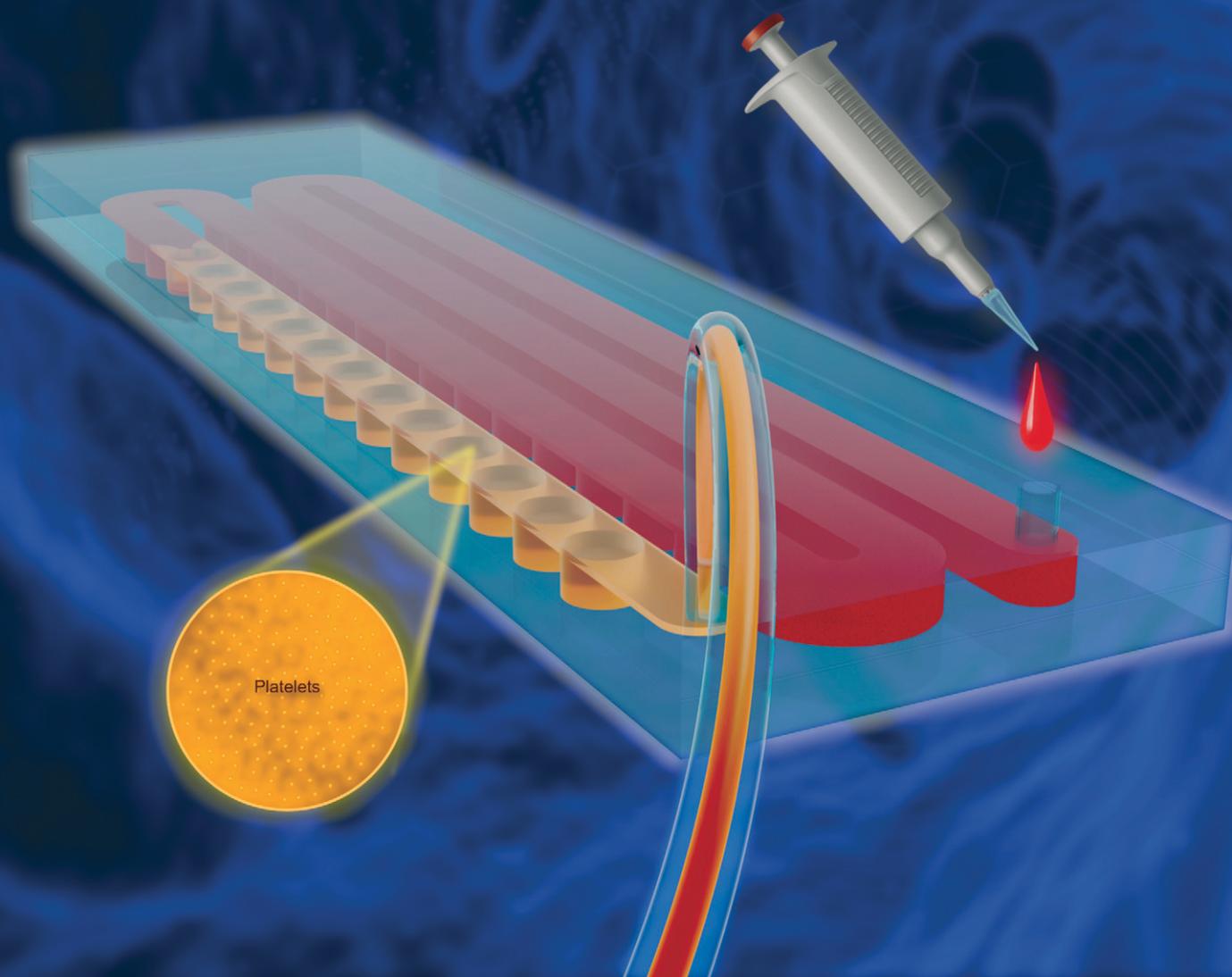
PAPER
Lourdes Basabe-Desmonts *et al.*
A microfluidic device for passive separation of platelet-rich
plasma from whole blood

Check for updates

A microfluidic device for passive separation of platelet-rich plasma from whole blood†

Pablo E. Guevara-Pantoja, [iD][a] Yara Alvarez-Braña,[ab] Jon Mercader-Ruiz,[ac] Fernando Benito-Lopez [iD][b] and Lourdes Basabe-Desmonts [iD] *[ad]

We present a microfluidic device for separating platelet-rich plasma (PRP) from whole blood, addressing key limitations in current sedimentation-based technologies. Unlike existing methods that rely on a single sedimentation trench—limiting plasma yield and processing speed—our device incorporates a novel multi-trench design, allowing the processing of 1 mL of whole blood in 40 minutes, yielding ~250 μL of PRP with at least a 2-fold increase in platelet concentration. The device is fabricated using a CO_2 laser cutter on acrylic layers and bonded with a pressure-sensitive adhesives, offering a cost-effective and simple alternative to more complex manufacturing processes. To ensure reliable PRP separation and minimize bubble formation, we applied a hydrophilic coating at the trench bottoms. We analyzed three trench geometries to optimize PRP yield and quality. Flow simulations optimized shear rates to improve sedimentation. Our approach effectively removes red and white blood cells with purities of 98% and 96%, respectively, only 8.2% of the total platelets were activated post-processing, compared to 31% with conventional centrifugation. This combination of a novel multi-trench layout, simplicity, cost-efficiency, and effective platelet preservation enables a low-cost device for obtaining high-quality PRP for clinical research and therapy.

1 Introduction

Platelets, red blood cells (RBC), white blood cells (WBC), and plasma are the main constituents of whole blood.[1] Platelets or thrombocytes are the smallest cells in blood and are responsible for hemostasis, by forming blood clots and secreting growth factors.[2] These discoid-shaped cells, typically 2–4 μm in diameter and 1 μm thickness, are found at concentrations between 1.5 and 4.5×10^5 μL^{-1} in the blood of healthy adults.[3]

Platelet separation from blood has several applications in clinical and research areas. Research lines studying platelet-related cardiovascular diseases,[4] diabetes,[5] cancer,[6] immunity,[7] inflammation,[7] sepsis,[8] *etc.*, often require the isolation of the platelets for their analysis. Platelet-rich plasma (PRP) is an autologous biological product derived from blood, used to treat various conditions by promoting tissue regeneration and repair.[9] PRP contains plasma with a platelet concentration higher than basal levels.[10] Clinics and hospitals need the separation and preparation of PRP for transfusions[11] or other applications including wound healing,[12] bone and tissue regeneration,[13] dental implants,[14] skin rejuvenation,[15] hair recovery,[16] fertility treatments,[17] *etc.*

The conventional methods for platelet isolation involve using an apheresis machine or the PRP and buffy coat double-spin centrifugation protocols.[18] While centrifuge methods are commonly used, they are complex due to their reliance on manual steps and labor-intensive processes.[19] Moreover, centrifugation can lead to blood contamination, low isolation reproducibility, and undesired platelet activation.[20–22] In fact, centrifugation may activate approximately 50% of total platelets.[23] Single-spin centrifugation methods offer the advantage of a simplified protocol for obtaining PRP; however, they may result in lower and less precise platelet concentrations compared to double-spin techniques.[24] There are also commercial single-spin systems, such as the Arthrex Angel System, RegenKit® (by RegenLab), and GPS® III System (by Biomet), but these can be costly and require specialized equipment. Thus, alternative methods are being explored to enhance efficiency and reduce platelet activation.

[a] *Microfluidics Cluster UPV/EHU, BIOMICs Microfluidics Group, Lascaray Research Center, University of the Basque Country UPV/EHU, 01006 Vitoria-Gasteiz, Spain. E-mail: lourdes.basabe@ehu.eus*

[b] *Microfluidics Cluster UPV/EHU, Analytical Microsystems & Materials for Lab-on-a-Chip (AMMa-LOAC) Group, University of the Basque Country UPV/EHU, Leioa, Spain. E-mail: fernando.benito@ehu.eus*

[c] *Advanced Biological Therapy Unit (UTBA), Hospital Vithas Vitoria, Vitoria-Gasteiz, Spain*

[d] *Basque Foundation of Science, IKERBASQUE, Bilbao, Spain*

† Electronic supplementary information (ESI) available. See DOI: https://doi.org/10.1039/d5lc00362h

Efforts have been made to develop technologies to obtain PRP preserving platelet integrity. For instance, a non-centrifugal method utilizing a polymeric sponge has been developed for platelet separation. This approach selectively absorbs platelets; however, it exhibits some contamination with RBCs (~60% platelets *vs.* RBC).[25] Microfluidics devices have been reported to offer advantages over conventional methods for platelet recovery.[22,26–28] Table S1† summarizes a review about microfluidic passive/active devices for platelets separation. In general, these microsystems are more portable, consume smaller sample volume, are amenable to automation, and notably induce lower platelet activation than conventional methods, as they exert less mechanical stress than high-speed centrifugation.[19] A notable example is a passive microfluidic device enabling platelet isolation with 40% less activation than a two-stage centrifugation protocol. This device processes whole blood up to 0.4 mL min⁻¹ and achieves 15-fold platelets enrichment.[28,29] However, its purity is only 50% in terms of platelets count relative to other blood cells. Another example is an active separation device that uses acoustic waves for high-throughput platelets isolation, processing whole blood at flow rates of 10.0 mL min⁻¹.[22] The device recovers platelets with just 7.8% activation, compared to 22% with centrifugation, and achieves 81.3% purity (platelets relative to other blood cells). However, its fabrication is complex, which may limit its widespread adoption.

There are also simple, passive microfluidic systems that use gravity sedimentation that demonstrate obtain high purity plasma from whole blood. Sedimentation by gravity is a straightforward method that exploits the density difference between plasma and blood cells. For instance, a device employing a trench to accelerate plasma separation achieves ~100% efficiency in red blood cell filtering when using whole blood.[30] Another device using enhanced gravity sedimentation using a trench geometry reports 99.9% efficiency in red blood cells filtration.[31] These sedimentation microsystems report higher purity compared to others (Table S1†); however, they are designed for small-scale plasma generation (a few μL min⁻¹) using a single-trench approach. Moreover, plasma separators based on sedimentation have never been studied in terms of platelet recovery and activation.

The design of a device for PRP extraction *via* sedimentation that incorporates multiple trenches could represent a promising solution to overcome the limited capacity of current trench-based microsystems, while preserving the high purity levels they achieve. One major drawback of trench-based separators is bubble formation, as blood often fails to completely fill the trench, reducing efficiency. Different strategies have been explored to mitigate bubbles, such as hydrophobic barriers,[30,32] degassing[33] and porous membranes.[34] However, these solutions introduce extra fabrication steps or require materials unsuitable for mass production.

Given the current state of the art in blood separation methods (Table S1†), a notable gap can be addressed by developing a microfluidic device specifically designed to efficiently prepare PRP from whole blood. Our objective is to achieve the production of pure PRP that is free from contaminants such as residual red blood cells or leukocytes. The device must be designed to operate in a closed system without the need for diluents or buffers, which could otherwise compromise the purity of the PRP or complicate its application. Additionally, a crucial innovation of this device should be its ability to preserve the quality of platelets by minimizing their activation during the separation process, in contrast to current methods that may inadvertently activate platelets, affecting their functionality and viability. Importantly, the device should function passively, relying solely on intrinsic fluidic forces rather than external power sources, and be easy to fabricate using cost-effective and scalable methods.

This work demonstrates a PRP separator from whole blood that utilizes gravity sedimentation as a working principle in a novel multi-trench device. The device consists of a blood reservoir and a microchannel with multiple rectangular, circular, or big trenches. Notably, this passive separator is easy to fabricate, as it is made from acrylic layers bonded with pressure-sensitive adhesives (PSA). A hydrophilic PSA is used at the bottom of the trenches to prevent bubble formation. Furthermore, the device is easy to handle, requiring only a syringe pump to both collect PRP and pump the blood. Extensive experiments were conducted using three different trench geometries to evaluate and compare PRP components, quantity, and separation dynamics. PRP separation in circular and rectangular trench devices was faster than in a big-trench device. Shear rate simulations were performed using the three devices at different flow rates and channel depths to determine the optimal conditions for blood sedimentation. As a result, PRP with a 2-fold increase in platelet concentration compared to baseline was obtained directly from undiluted whole blood with 98% purity at a flow rate of 12.5 μL min⁻¹. Finally, platelet activation was measured, showing better platelet integrity when using the developed devices compared to the conventional centrifugation method. This development can pave the way for obtaining high-quality PRP using a simple and low-cost passive method.

2 Materials and methods

2.1 Fabrication and assembly

2.0 mm-thick poly(methyl methacrylate) (PMMA) sheets (ME303020/20, Good Fellow, UK) were cut and carved using a laser system (VLS2.30 Desktop Universal Laser System, VERSA Laser, USA) equipped with a 10.6 μm CO_2 laser source, operating at a power range of 10 to 30 W. Trenches, flow channels, and holes were fabricated on two acrylic layers (flow layer and cover layer). Measurements were performed using a profilometer (DektakXT, Bruker, USA). Channels and

trenches created under different laser system conditions were characterized to determine the exact parameters required to achieve a depth between 100 and 400 μm, as needed. Irregularities caused by laser cutting were removed before assembling the acrylic layers using abrasive paper (734-P800, 3M, Italy). The assembly process was as follows: (i) the flow layer and the cover layer were manually aligned and bonded with a transparent double-sided pressure-sensitive adhesive (PSA) (ARcare 90880, Adhesive Research). (ii) The bottom of the trenches was sealed with a hydrophilic PSA (ARflow 93049, Adhesive Research, USA) and pressed with a hand roller until a completely transparent and bubble-free layer was observed, ensuring proper sealing. (iii) Finally, 1.5 mm outer diameter Tygon tubes (AAD04103, Saint Gobain, USA) were glued (Loctite 495, Henkel, USA) to the chip's inlets for fluid handling (Fig. S1†)

2.2 Shear rate and velocity simulations

Numerical analysis was performed in COMSOL using the Laminar Flow Module and the Carreau model for non-Newtonian fluids to describe the viscosity as a function of shear rate of whole blood.[35,36] The 3D model of the device with separation trenches was imported from AutoCAD 2023 as a CAD file. The liquid properties were those reported for whole blood using the Carreau model: a density (ρ) of 1050 kg m^{-3}, zero shear viscosity (μ_0) of 0.056 Pa s, high shear viscosity (μ_∞) of 0.0035 Pa s, characteristic time (λ) of 3.313 s and exponent (n) of 0.3568. The generated mesh consisted of tetrahedral elements with a calibrated size, a maximum and minimum element size of 40 and 1.5 μm, respectively, and a maximum element growth rate of 1.3. The wettability of the materials was configured as follows: PMMA with a contact angle of 60°, hydrophilic PSA with a contact angle of 6° and normal PSA with a contact angle of 90°. Simulations of the devices were performed using four different channel depths (100, 200, 300, and 400 μm) and three different flow rates (12.5, 25.0, 50.0 μL min^{-1}). Thus, we performed 12 simulations in total, three for each channel depth.

2.3 Filling studies

The correct filling of the device is necessary to avoid bubbles; this depends on the properties of the material and the geometry of the channels. To study how materials affect this, devices were prepared using hydrophilic and hydrophobic PSA at the bottom of the separation trenches for the three device designs. Images taken during device filling at a 50.0 μL min^{-1} flow rate using a smartphone (12 megapixels, iPhone, USA) were used to measure bubble formation. Red food dye in distilled water was used for these experiments.

2.4 PRP separation

Blood was obtained from three healthy male individuals aged between 25 and 60. All experiments were conducted in accordance with the Declaration of Helsinki (Fortaleza, Brazil; 2013) and the CIOMS International Ethical Guidelines for Health-related Research Involving Humans (2016). The study protocol was approved by the Ethics Committee of the University of the Basque Country (UPV/EHU; Ref. 2019-234, 13 May 2020). Written informed consent was obtained from all participants prior to inclusion in the study. Blood samples were obtained via venous puncture in 9 mL tubes containing sodium citrate as an anticoagulant. Blood was collected on the same day as the experiments to ensure freshness. PRP was separated from the blood by sedimenting the RBC using the trench-based device. Before each PRP separation experiment, 1 mL of whole blood was injected into the chip reservoir by pipetting. A syringe pump (Pump 11 Elite, Harvard Apparatus, USA) in withdrawal mode, equipped with a 1 mL disposable syringe, was connected to the outlet to collect the separated PRP and impose flow rates of 12.5, 25.0, 37.5, and 50.0 μL min^{-1}, depending on the test condition. The separation experiment concludes when the RBC reached the outlet of the chip. Competent and trained personnel handled and processed patient samples following the institutional security protocols.

2.5 PRP characterization

Components of whole blood and extracted PRP were measured to calculate separation purity, platelet concentration, and WBC concentration. The blood and PRP samples used in the experiments were analyzed using a hematologic analyzer (XS-1000i, Sysmex, JP). Samples were kept at 2–8 °C until analysis. During the experiments, images of PRP separation were taken for analysis using a smartphone camera (12 megapixels, iPhone, USA). The images were analyzed using ImageJ software. An intensity profile of a line at the center of the separation channel was acquired to track the progression of the liquid meniscus of blood and PRP over time. Then, the PRP generation dynamics were calculated based on the meniscus progression and the channel dimensions.

2.6 Platelets activation assay

Anti-CD62p antibodies tagged with phycoerythrin (PE) (561921, BD, USA) and anti-CD41A antibodies tagged with fluorescein isothiocyanate (FITC) (561851, BD, USA) were used as markers for platelet activation. The PRP obtained from the experiments was prepared as follows: first, an antibody cocktail consisting of 5 μL of anti-CD62p and 5 μL of anti-CD41A was diluted in 80 μL of PBS (Gibco pH 7.4, Fisher Scientific, USA) for each sample analysis. Then, 10 μL of PRP samples were mixed with the antibody solution and incubated for 15 minutes in the dark. Next, platelets were fixed with a 1.25% solution of formaldehyde in PBS, prepared from a 4% formaldehyde reagent (15423179, Fisher Scientific, USA). Finally, a ten-color flow cytometer (Gallios, Beckman Coulter, IE) was used for sample analysis. Data were analyzed using Gallios 1.2

software. The centrifugal method used for comparison was the PRGF Endoret single-spin protocol. 9 mL tubes were centrifuged at $580 \times g$ (the time for centrifugation ascent and descent is not stated by the provider). 2 mL of plasma above the buffy coat were collected.

2.7 Data analysis

The experimental data was plotted and analyzed in Prism 6 (GraphPad Software, USA). Means comparisons were done using independent samples t-test or z-test depending on the sample size and variance assumptions. A p-value < 0.05 was considered indicative of statistical significance.

3 Discussion and results

3.1 Microfluidic device

Our PRP separator consists of multiple traps or trenches interconnected by a fluidic microchannel. Three different trench geometries were studied to observe how the resultant PRP's quantity, composition, and quality are affected after processing whole blood. Fig. 1a shows the three studied devices: the first has fifty rectangular trenches ($1.5 \times 3 \times 2$ mm), the second has thirty-two circular trenches (3 mm in diameter), and the third has two big trenches ($40 \times 3 \times 2$ mm). Identical dimensions were used for the interconnecting microchannel ($135 \times 3 \times 0.3$ mm) and the number of trenches was adjusted to maintain a similar dead volume, ensuring
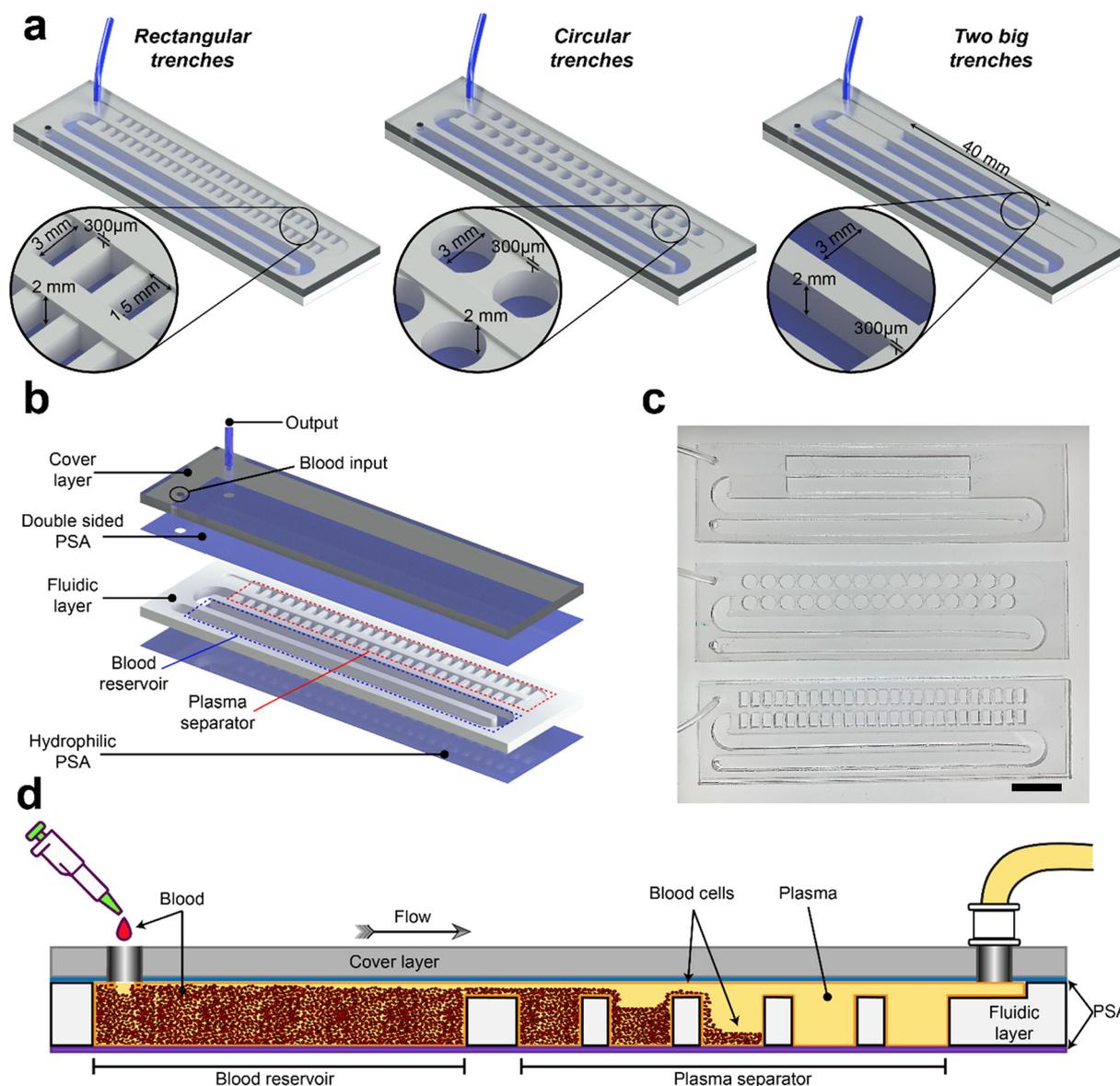
Fig. 1 Design of the different PRP separator devices. a) Geometries used for the devices with rectangular, circular, and big trenches. b) Exploded view showing the components of the device with rectangular trenches. c) Photograph of the real devices made of transparent acrylic. Scale bar of 1 cm. d) Schematic show the sedimentation process that occurs along the microfluidic device, from the blood reservoir to the PRP separator and collector.

Paper

comparative results between the three designs. Specifically, the internal or dead volume of the PRP separator is 502 μL for the circles design, 499.3 μL for the rectangles design, and 525.3 μL for the big trenches design. The devices were designed so that this volume would approximately match the total volume occupied by red blood cells in one milliliter of whole blood, which is about 45–55% of the total volume. A possible limitation of this design is that it operates in a batch-type processing mode, which means it cannot handle blood volumes greater than 1 mL. This is because, once saturated, the trenches lose their capacity to capture red blood cells. To increase the processing capacity, it would be necessary to either increase the number of trenches or modify their dimensions.

Fig. 1b shows an exploded view of the different layers of our devices. Each device consist of a fluidic layer and cover layer bonded by double-sided PSA and sealed at the bottom of the trenches with a hydrophilic PSA film. The fluidic layer, which is the most complex, contains the trenches, the fluidic microchannel, and the blood reservoir. The cover layer includes the inlet for pipette, the blood and the outlet tube to connect the syringe pump. The blood reservoir, capable of

holding 1 mL of blood, is integrated into the device to improve the reproducibility of PRP separation. Fig. 1c shows the three fabricated devices, each with dimensions of 20 mm × 80 mm × 4 mm. The separation process is outlined in Fig. 1d. Briefly, the syringe pump draws blood from the on-chip reservoir into the separation trenches, where the blood flows through the microchannel and trenches, and the RBC/WBC cells sediment due to their higher density. The RBC/WBCs are captured at the bottom of the trenches because of their low-velocity flow profile. Finally, the separated PRP is collected in the syringe.

3.2 Shear rate and velocity simulations

Approximately 45–55% (v/v) of whole blood consist of red blood cells (RBCs).[1] Separation of plasma from RBCs *via* gravity sedimentation primarily occurs due to the slightly higher density of RBCs compared to plasma (1.13 g mL^{-1} for RBCs and 1.03 g mL^{-1} for plasma). In addition to the density difference, sedimentation can be enhanced by the formation of RBC clumps through the Rouleaux effect.[37] However, this effect only occurs at low shear rates. At shear rates above 50
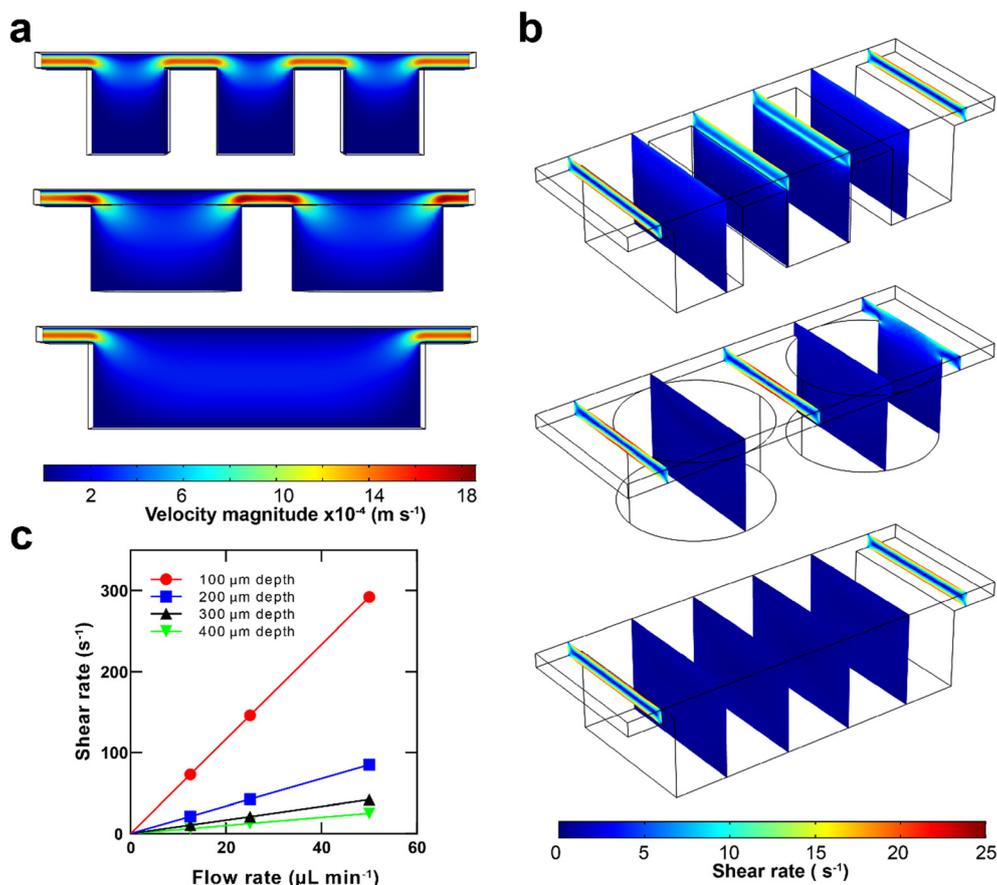

Fig. 2 Shear rate and velocity simulations. a) Simulations of flow velocities of the rectangular (top), circular (middle) and big (bottom) trenches devices using a microchannel of 300 μm in depth and a flow rate of 50.0 μL min^{-1}. b) Simulations of the shear rate of the rectangular (top), circular (middle) and big (bottom) trenches devices using a microchannel of 300 μm in depth and a flow rate of 50.0 μL min^{-1}. c) Results of shear rate simulations at different flow rates (12.5, 25.0 and 50.0 μL min^{-1}) of a rectangular trench device using 100, 200, 300, and 400 μm in depth microchannel.

s^{-1}, the shear field disrupts aggregation, while at lower shear rates, RBCs can reversibly aggregate. RBC aggregation significantly increases the settling rate, as the settling rate of particles depends on the square of their size. To determine the shear rate in the devices, numerical analyses were performed to identify the conditions for a fast sedimentation rate of RBCs. Simulations of three designs, using four interconnection channels of different depths, were conducted. Fig. 2a shows the flow velocity field for the central slide of the three designs at a flow rate of 50.0 μL min^{-1}, with the maximum velocity observed in the interconnection channel. Fig. 2b shows the shear rates for the three devices under the same velocity conditions. As expected, the maximum shear rate was observed between the trenches in the microchannels, as it is proportional to the flow velocity, and this transverse section in the device has the highest flow velocity. Results from simulations at flow rates of 12.5, 25.0, 37.5, and 50.0 μL min^{-1} using microchannels with depths of 100, 200, 300, and 400 μm are shown in Fig. 2c. Microchannels with depths of 100 and 200 μm generated shear rates above 50 s^{-1} for several of the studied flow rates, which may reduce RBC aggregation and result in a lower performance plasma separator. On the other hand, microchannels with depths of 300 and 400 μm did not exceed the shear rate of 50 s^{-1}, making them suitable for this application as they allow RBC aggregation. Thus, the device with a 300 μm channel depth was chosen due to its compatibility with RBC aggregation and its lower dead volume compared to the 400 μm channel, as a device generating minimal waste is desired.

3.3 Filling studies

Trench devices suffer from bubble formation due to abrupt dimensional changes in their fluidic paths. Several strategies have been employed to address this issue, such as the use of hydrophobic barriers,[30,32] degasification,[33] or porous membranes.[34] The device utilizes a simpler approach to prevent bubble formation by employing a hydrophilic PSA at the bottom of each trench (contact angle of 6–7°). Regular PSAs are inherently hydrophobic (contact angle >90°);[38] however, hydrophilic PSA compositions have recently been developed.[39] The primary distinction between using hydrophilic and regular PSAs lies in the liquid's flow behavior within the trench. Fig. 3a illustrates the filling differences in an individual circular trench using regular and hydrophilic PSAs at the bottom. With regular PSA, the liquid moves along the PMMA walls and the top layer, as these surfaces are already in contact with the flowing liquid. Eventually, the liquid reaches the bottom; however, the hydrophobic nature of the regular PSA hinders a homogeneous and reproducible filling of the trench. This irregular filling results in bubble formation in several trenches of the device (Fig. 3a, after filling). In contrast, when using the hydrophilic PSA, the liquid readily wets and flows across the bottom of the trench, enabling a more controlled filling from bottom to top. The same filling behavior was observed with the rectangular and big trench devices. Fig. 3b presents a bar chart comparing the percentage of trenches containing bubbles for both PSA methods, demonstrating that the hydrophilic PSA effectively mitigates bubble formation. Thus, by utilizing the hydrophilic PSA, the filling of each trench becomes
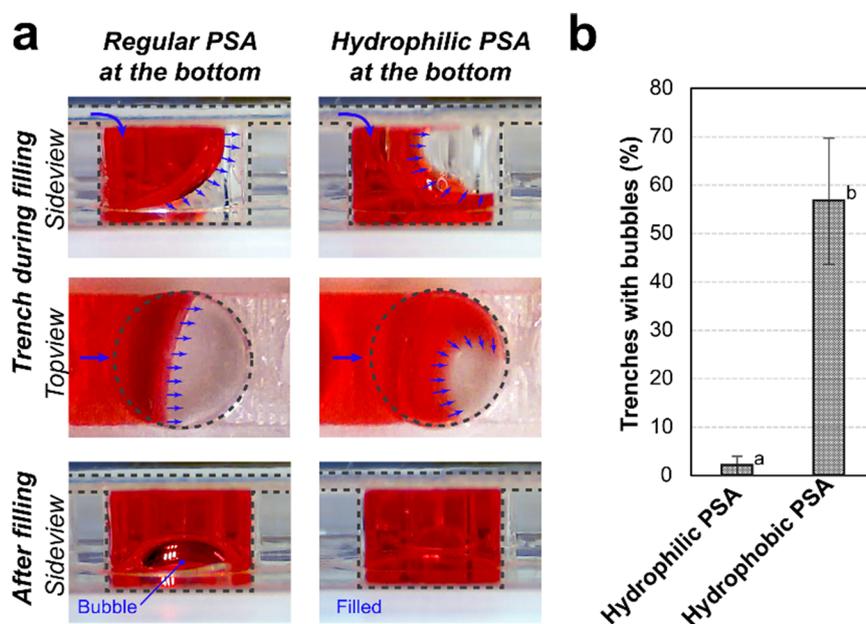
Fig. 3 A circular trench of 3 mm of diameter during and after filling it with red colorant. a) On the left, images of the filling using regular PSA in the bottom of the trench, and on the right using hydrophilic PSA. b) Bubble formation in devices with hydrophilic and hydrophobic pressure-sensitive adhesives (PSA) at the bottom of the trenches. $N = 150$ trenches from three devices. Error is S.D. Different letters (a and b) indicate significant statistical difference ($p < 0.005$, z-test).
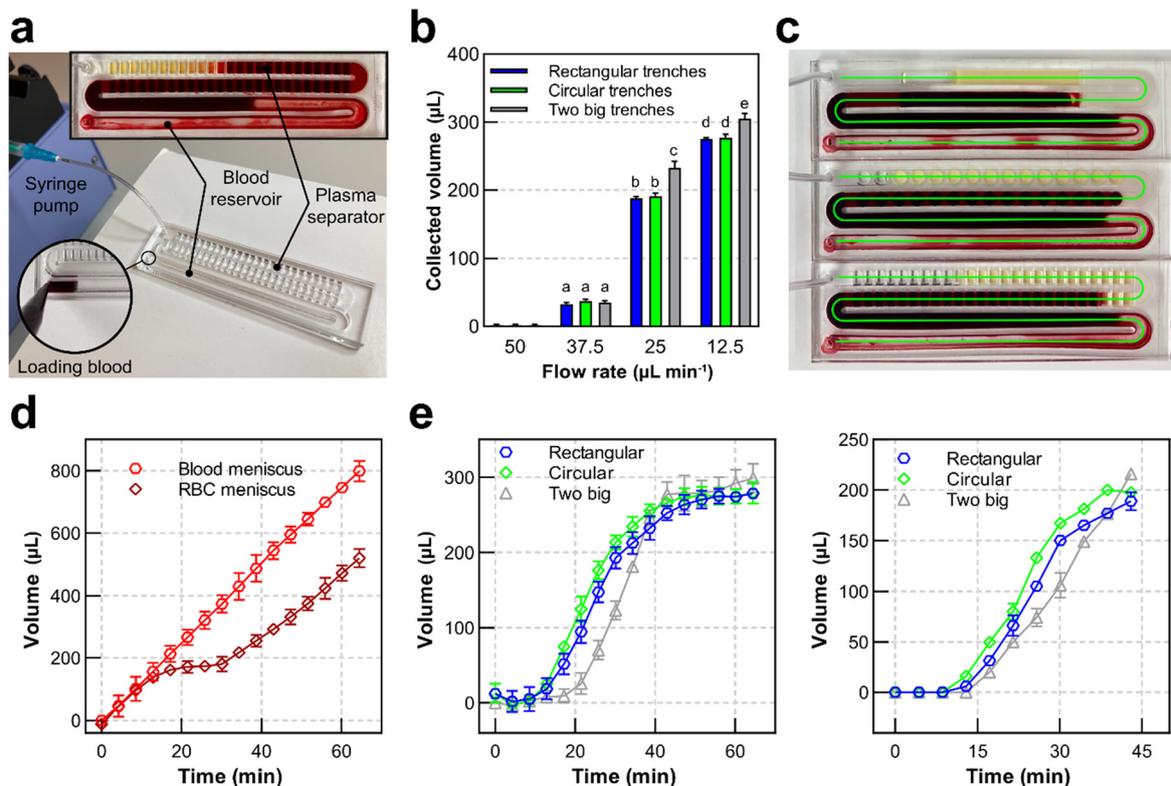
Fig. 4 PRP separation results. a) Experimental setup to study the PRP separation of the trenches devices. b) Collected volume of PRP of the rectangular, circular, and big trenches devices at different flow rates. c) Real photograph during a separation experiment shows the green line used for the analysis of PRP generation dynamics. d) Volume progress over time, of the whole blood meniscus (in red) and the RBC meniscus (in brown) during a separation experiment using the rectangular trenches device. e) Volume progress over time, of PRP generation during an experiment using the three device designs at flow rates of 12.5 μL min⁻¹ (left) and 25.0 μL min⁻¹ (right). All charts show mean and S.D. values. N = 3. Distinct letters (a–e) signify $p < 0.05$, t-test.

reproducible and reliable, resulting in PRP separation devices that are easy to fabricate and free of bubbles.

3.4 PRP separation

The device was initially designed to process 1 mL of whole blood to evaluate its performance and the quantity and quality of the PRP yield. Fig. 4a shows the setup for a PRP separation experiment using the device with rectangular trenches. For each PRP separation assay, 1 mL of whole blood was pipetted into the device before connecting the tube to the syringe pump, allowing the purging of air from the system. We tested four flow rates (12.5, 25.0, 37.5, and 50.0 μL min⁻¹) for each of the three designs and measured the volume of PRP collected in the syringe after each experiment. We observed that the collected PRP volume was inversely proportional to the flow rate, with a maximum of 300 μL obtained at 12.5 μL min⁻¹ (Fig. 4b). Experiments at lower flow rates required more time; for instance, at 12.5 μL min⁻¹, the process took 65 min, compared to 30 min and 15 min for flow rates of 25.0 and 37.5 μL min⁻¹, respectively. No PRP separation was observed at 50.0 μL min⁻¹. This variation in assay duration is likely the primary factor affecting the collected PRP volume, as lower flow rates allow more time for

blood sedimentation inside the PRP separator. Additionally, significant differences in PRP yield were observed among the device designs at the same flow rates. While the devices with rectangular and circular trenches produced comparable PRP volumes, the device with two big trenches collected approximately 11% and 6% more PRP at 25.0 and 12.5 μL min⁻¹, respectively. This difference in collected volume is likely due to an agitation effect caused by the abrupt changes in cross-sectional area in the rectangular and circular trench designs, a phenomenon absents in the big-trench device. Overall, we demonstrate that the devices can effectively separate PRP from whole blood at different flow rates with high reproducibility.

Our findings demonstrate that the multi-trench design generates significantly more PRP than single-trench devices.[30,31] If a higher volume is required, increasing the number of trenches could enable greater blood processing capacity, either by integrating multiple devices in series or parallel. However, further research is needed to optimize this approach. Additionally, the total processing time for PRP using our device is comparable to conventional protocols, which involve two centrifugation steps along with multiple collection and resuspension steps, typically requiring 30–40 minutes.[40] Moreover, our device achieves a PRP recovery

efficiency of 25% (250 μL of PRP from 1 mL of whole blood in 40 minutes), which is substantially higher than the 10–15% efficiency typically reported for centrifugation-based methods.[40]

Image analysis of PRP separation videos was performed to elucidate the dynamics of PRP generation during a complete experiment. Fig. 4c shows a video frame with the green line used to identify the position of whole blood and the RBC meniscus in the flow channel. This position can be converted to volume using the known dimensions of the channel and trenches. The progression of whole blood (in red) and RBCs (in brown) over time is shown in Fig. 4d. As expected, the whole blood flow (red plot line) increased linearly over time, with a linear trend line (R^2 = 0.9997) and a slope of 12.54, consistent with the 12.5 μL min^{-1} flow rate set on the syringe pump. This confirms the desired blood flow rate through the PRP separator and its stability during experiments. In contrast, the RBC meniscus (brown plot line) is affected by sedimentation and the trenches of the PRP separator, resulting in a velocity slowdown after the first 10 minutes. However, RBC flow recovers 80% of its initial rate after 30 minutes and eventually reaches the same velocity as whole blood, indicating the completion of PRP separation. The difference between the whole blood and RBC meniscus positions corresponds to the PRP volume generated over time. This dynamic PRP generation can be calculated for each device design at different flow rates (Fig. 4e). For experiments at 12.5 μL min^{-1} (Fig. 4e, left), similar PRP generation dynamics were observed between devices with rectangular and circular trenches, while the device with big trenches exhibited a 10-minute delay before PRP generation began. At 25.0 μL min^{-1} (Fig. 4e, right), no significant differences were observed between trench designs. Image analysis could not be performed for the 37.5 and 50.0 μL min^{-1} experiments due to the very low or absent PRP generation. Interestingly, despite the difference in flow rates, the 12.5 and 25.0 μL min^{-1} experiments generated similar PRP volumes over time. For example, at 30 minutes, both

had separated approximately 200 μL of PRP. This suggests that PRP generation depends more on sedimentation time inside the device than on flow rate.

3.5 PRP composition

The whole blood is primarily composed of plasma, red blood cells (RBCs), white blood cells (WBCs), and platelets. We characterized the PRP obtained from the devices to assess its separation purity and the concentrations of other components. Fig. 5a (right) presents the concentrations above baseline values (expressed as a percentage of whole blood baseline concentrations) for WBCs, RBCs, and platelets across the three device designs, using whole blood from the same patient. Assay reproducibility was observed, with maximum coefficient of variability (CV) values of 32%, 24%, and 8% for WBCs, RBCs, and platelets, respectively. Regarding RBC removal, we observed average values of 99.4% for both the square and circular trench devices, and 99.6% for the large trench device. For WBC removal, the average values were 59.7%, 68.3%, and 94% for the square, circular, and large trench devices, respectively. The PRP purity, defined as the proportion of platelets relative to all other cellular components—explicitly accounting for residual RBCs and WBCs—was calculated as 92.13%, 93.1%, and 93.2% for the square, circular, and large trench devices, respectively. Interestingly, platelets were concentrated 2.5-fold across all three device designs, likely due to the elimination of RBC occupancy volume.

In experiments using samples from three different patients (Fig. 5a, left), we observed CV values of 74%, 25%, and 21% for WBCs, RBCs, and platelets, respectively, while still maintaining high purity and efficient RBC removal across all samples. This greater variability is likely attributed to significant differences in blood composition between individuals. In this case, the device was able to obtain PRP with a platelet concentration twice the baseline, corresponding to approximately 400 000 platelets per
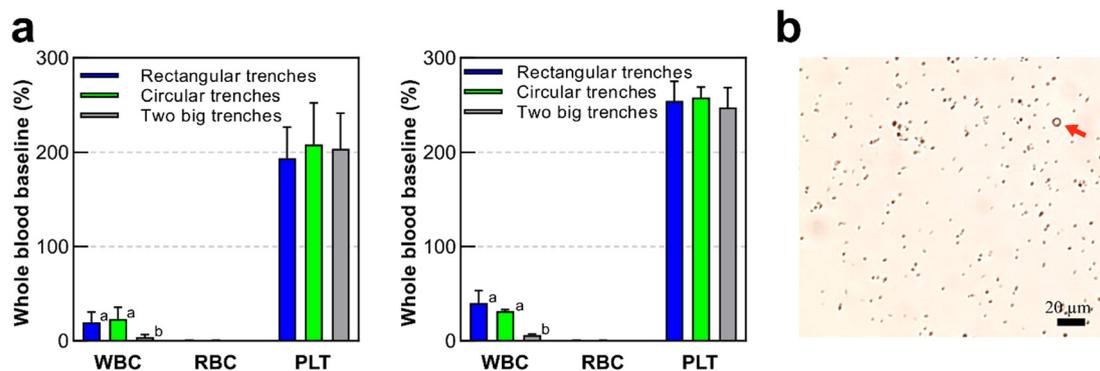
Fig. 5 PRP composition. a) Hematologic analyzer results of PRP samples collected from the three device types after processing the same whole blood sample (at the left) or after processing three different whole blood samples (at the right) for white blood cells (WBC), red blood cells (RBC), and platelets (PLT). Mean and S.D. above baseline values (% of basal concentrations of whole blood), N = 3. Different letters (a and b) indicate significant statistical difference ($p < 0.05$, t-test). b) Micrograph of a device collected PRP sample showing platelets and a RBC as size reference (red arrow).

Paper

microliter, which falls within the definition of PRP. While PRP with platelet concentrations of at least 1 million platelets per microliter is typically used in applications such as odontology,[41] orthopedics,[42] and sports medicine,[43] PRP with concentrations of 400 000 platelets per microliter also has practical applications in ophthalmology,[44] aesthetic medicine,[45] and superficial wound healing.[20]

No significant differences in PRP composition were observed between the rectangular, circular and big-trench devices for PTL and RBC; however, the big-trench devices exhibited a significant reduction of WBC concentration compared to the others. This difference may be due to the longer trenches allowing WBC sedimentation alongside RBCs, whereas devices with smaller trenches likely retained WBCs in suspension due to abrupt flow rate changes. It is important to note that there is a significant distinction between PRP rich in WBCs (LR-PRP) and WBC-free PRP (LP-PRP), each with its own advantages and disadvantages depending on the application. For instance, in knee osteoarthritis, LP-PRP has been shown to significantly improve WOMAC scores (pain, disability, and joint stiffness) compared to LR-PRP. The biological basis for this effect may be linked to differences in the levels of inflammatory and anti-inflammatory mediators in LR-PRP and LP-PRP.[46] Fig. 5b shows a micrograph of a PRP sample obtained from the device with rectangular trenches. Furthermore, the design of our device allows for the integration of additional sample processing steps to further concentrate platelets if required, such as incorporating hydrogel beads to absorb water,[9] ultrafiltration,[47] or evaporation.[48]

3.6 Platelets activation

As observed, the devices can separate PRP while maintaining platelet concentrations twice as high as the basal concentration in whole blood. The plasma quality is related to platelet activation especially when preparing PRP. To assess platelet quality, we performed platelet activation assays using three different device designs with three independent whole-blood samples. For comparison, platelet activation levels were also measured in samples processed by a conventional centrifugation method. The activation levels of both methods were compared by measuring the expression of P-selectin (CD62p), a commonly used marker of platelet activation.[49] Flow cytometry was used to analyze the samples, with platelets labeled using anti-CD62p antibodies conjugated with PE and anti-CD41 antibodies conjugated with FITC as a positive control to identify all platelets. Fig. 6a presents a representative flow cytometry result showing platelet fluorescence levels. Fig. 6b summarizes the platelet activation results for the three device designs and the centrifugation method, demonstrating that all device designs induce lower platelet activation than centrifugation. In average we found only 13.5% of the total platelets were activated for the rectangular or circular trenches and 12.7% for the big trenches, significantly low compared to 31% in the centrifugation method. Considering that venipuncture and collection in citrate tubes alone can result in approximately 5% platelet activation,[50,51] and our devices showed an average total activation of ~13%, we estimate that approximately 8% of the platelets are activated specifically within the chip. This suggests that platelets experience low mechanical stress within the devices.

It is well established that platelet activation requires shear rates of at least 1000 s^{-1}.[52] Since our device operates at shear rates below 50 s^{-1}, these values remain within the physiological range and are unlikely to induce platelet activation.[53] The activation observed in our results is likely due to the extraction method and the time within the chip which is >30 min. In contrast, centrifugation can cause irreversible changes in platelet morphology and function, potentially limiting their therapeutic applications.[19]

4 Conclusions

We have successfully developed a microfluidic device tailored for the separation of PRP from whole blood. While other methods and devices for blood and plasma
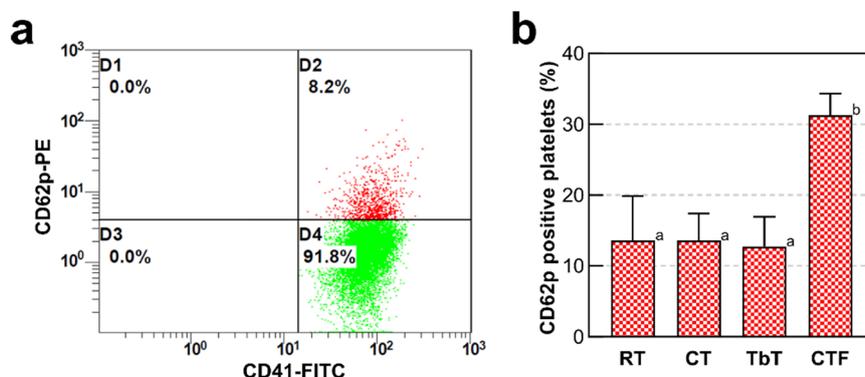

Fig. 6 Platelets activation assay. a) Representative result of flow cytometry showing the total platelets (D2 and D4) and the activated platelets (D2). b) Summary of the platelets activation results for the rectangular (RT), circular (CT) and two big (TbT) trenches devices along with the centrifugation method (CTF). Error is S.D. N = 3. Different letters (a and b) indicate significant statistical difference (p < 0.05, t-test).

separation exist, this study addresses a critical gap by focusing on the development of a device designed to efficiently produce PRP with minimal platelet activation. Our device eliminates contaminants such as residual red blood cells and leukocytes from whole blood, operating solely with a syringe pump and without the need for diluents or buffers that could compromise PRP purity or complicate its use. Crucially, the device's novel design preserves platelet quality by minimizing activation during separation, in contrast to conventional methods that may inadvertently activate platelets.

The device consists of several acrylic layers, carved by a CO_2 laser and bonded with PSA, ensuring straightforward fabrication and assembly. Numerical simulations were instrumental in optimizing the design to enhance red blood cell sedimentation, permitting the Rouleaux phenomenon, which occurs only at specific shear rates. Although the current device is designed to process 1 mL of whole blood, it could potentially be scaled up to handle larger volumes with minimal modifications. Furthermore, connecting multiple chips in parallel may offer a viable strategy to increase the total volume of plasma collected, thereby enhancing its suitability for a variety of clinical PRP applications. Moreover, our device, with the capacity to separate 250 μL of PRP, already outperforms similar single-trench devices by producing several times more PRP while maintaining high purity, positioning it as a promising tool for applications such as biomarker detection, platelet assays, or cell culture assays.

Additionally, the syringe pump could be replaced by other affordable pumping systems, such as PDMS vacuum pumps,[54] acrylic micropumps,[55] low-cost peristaltic pumps,[56,57] or an open-source syringe pump.[57] We consider it feasible to develop a dedicated instrument to operate cartridges incorporating the PRP separator. These cartridges can be fabricated using the method described here or through scalable mass-production techniques, as the device is made from thermoplastics compatible with such processes. Overall, our microfluidic device provides a straightforward solution for efficiently obtaining high-quality PRP, with advantages in fabrication simplicity, scalability, and operational adaptability. It minimizes the risk of contamination and eliminates the need for sterile operating facilities, as it operates as a closed system.

Data availability

The authors of this manuscript declare that all the data used will be provided under reasonable request to the corresponding author Lourdes Basabe Desmonts: lourdes.basabe@ehu.eus.

Conflicts of interest

There are no conflicts to declare.

References

1 Y.-C. Fung, Mechanical Properties of Living Tissues, *Biomechanics*, Springer, New York, 2nd edn, 1993, pp. 66–105.

2 L. Basabe-Desmonts, S. Ramstrom, G. Meade, S. O'neill, A. Riaz and L. P. Lee, *et al.*, Single-Step Separation of Platelets from Whole Blood Coupled with Digital Quantification by Interfacial Platelet Cytometry (iPC), *Langmuir*, 2010, **26**, 14700–14706.

3 R. J. Liesner and S. J. Machin, ABC of clinical haematology: Platelet disorders, *BMJ*, 1997, **314**, 809.

4 S. Willoughby, A. Holmes and J. Loscalzo, Platelets and Cardiovascular Disease, *Eur. J. Cardiovasc. Nurs.*, 2002, **1**, 273–288.

5 F. Santilli, P. Simeone, R. Liani and G. Davì, Platelets and diabetes mellitus, *Prostaglandins Other Lipid Mediators*, 2015, **120**, 28–39.

6 G. F. Nash, L. F. Turner, M. F. Scully and A. K. Kakkar, Platelets and cancer, *Lancet Oncol.*, 2002, **3**, 425–430.

7 C. N. Jenne and P. Kubes, Platelets in inflammation and infection, *Platelets*, 2015, **26**, 286–292.

8 S. F. Stoppelaar, C. van 't Veer and T. Van der Poll, The role of platelets in sepsis, *Thromb. Haemostasis*, 2014, **112**, 666–677.

9 J. Mercader Ruiz, M. Beitia, D. Delgado, P. Sánchez, M. J. Arnaiz and L. López de Dicastillo, *et al.*, New Formulation of Platelet-Rich Plasma Enriched in Platelet and Extraplatelet Biomolecules Using Hydrogels, *Int. J. Mol. Sci.*, 2023, **24**, 13811.

10 J. Mercader-Ruiz, M. Beitia, D. Delgado, P. Sánchez, B. Porras and I. Gimeno, *et al.*, Current Challenges in the Development of Platelet-Rich Plasma-Based Therapies, *BioMed Res. Int.*, 2024, **2024**, 6444120.

11 A. Holbro, L. Infanti, J. Sigle and A. Buser, Platelet transfusion: basic aspects, *Swiss Med. Wkly.*, 2013, **143**, 13885–13885.

12 P. Oneto and J. Etulain, PRP in wound healing applications, *Platelets*, 2020, **32**, 189–199.

13 I. A. Rodriguez, E. A. Growney Kalaf, G. L. Bowlin and S. A. Sell, Platelet-rich plasma in bone regeneration: Engineering the delivery for improved clinical efficacy, *BioMed Res. Int.*, 2014, **1**, 392398.

14 A. Albanese, M. E. Licata, B. Polizzi and G. Campisi, Platelet-rich plasma (PRP) in dental and oral surgery: From the wound healing to bone regeneration, *Immun. Ageing*, 2013, **10**, 1–10.

15 M. Banihashemi and S. Nakhaeizadeh, An introduction to application of platelet rich plasma (PRP) in skin rejuvenation, *RCM.*, 2014, **1**, 38–43.

16 G. Dervishi, H. Liu, S. Peternel, A. Labeit and F. Peinemann, Autologous platelet-rich plasma therapy for pattern hair loss: A systematic review, *J. Cosmet. Dermatol.*, 2020, **19**, 827–835.

17 P. Melo, C. Navarro, C. Jones, K. Coward and L. Coleman, The use of autologous platelet-rich plasma (PRP) versus no intervention in women with low ovarian reserve undergoing fertility treatment: a non-randomized interventional study, *J. Assist. Reprod. Genet.*, 2020, **37**, 855–863.

18 E. Vasconcelos, A. C. Figueiredo and J. Seghatchian, Quality of platelet concentrates derived by platelet rich plasma, buffy coat and Apheresis, *Transfus. Apher. Sci.*, 2003, **29**, 13–16.

19 V. Laxmi, S. Tripathi, S. S. Joshi and A. Agrawal, Microfluidic Techniques for Platelet Separation and Enrichment, *J. Indian Inst. Sci.*, 2018, **98**, 185–200.

20 D. M. Dohan Ehrenfest, L. Rasmusson and T. Albrektsson, Classification of platelet concentrates: from pure platelet-rich plasma (P-PRP) to leucocyte- and platelet-rich fibrin (L-PRF), *Trends Biotechnol.*, 2009, **27**, 158–167.

21 W. S. Nesbitt, E. Westein, F. J. Tovar-Lopez, E. Tolouei, A. Mitchell and J. Fu, *et al.*, A shear gradient–dependent platelet aggregation mechanism drives thrombus formation, *Nat. Med.*, 2009, **15**, 665–673.

22 Y. Chen, M. Wu, L. Ren, J. Liu, P. H. Whitley and L. Wang, *et al.*, High-throughput acoustic separation of platelets from whole blood, *Lab Chip*, 2016, **16**, 3466–3472.

23 A. C. Söderström, M. Nybo, C. Nielsen and P. J. Vinholt, The effect of centrifugation speed and time on pre-analytical platelet activation, *Clin. Chem. Lab. Med.*, 2016, **54**, 1913–1920.

24 T. Kawase, Platelet-rich plasma and its derivatives as promising bioactive materials for regenerative medicine: basic principles and concepts underlying recent advances, *Odontology*, 2015, **103**, 126–135.

25 L. H. Huang, C. S. Rau, W. H. Zeng, T. H. Lu, Y. C. Wu and Y. H. Chiu, *et al.*, A new technique for separating platelet-rich plasma by a copolymer device - without a centrifugation process, *Biomed. Pharmacother.*, 2022, **153**, 113481.

26 M. S. Pommer, Y. Zhang, N. Keerthi, D. Chen, J. A. Thomson and C. D. Meinhart, *et al.*, Dielectrophoretic separation of platelets from diluted whole blood in microfluidic channels, *Electrophoresis*, 2008, **29**, 1213–1218.

27 J. Nam, H. Lim, D. Kim and S. Shin, Separation of platelets from whole blood using standing surface acoustic waves in a microchannel, *Lab Chip*, 2011, **11**, 3361–3364.

28 V. Laxmi, S. S. Joshi and A. Agrawal, Design Evolution and Performance Study of a Reliable Platelet-Rich Plasma Microdevice, *Ind. Eng. Chem. Res.*, 2020, **59**, 20515–20526.

29 V. Laxmi, S. Tripathi, S. S. Joshi and A. Agrawal, Separation and Enrichment of Platelets from Whole Blood Using a PDMS-Based Passive Microdevice, *Ind. Eng. Chem. Res.*, 2020, **59**, 4792–4801.

30 I. K. Dimov, L. Basabe-Desmonts, J. L. Garcia-Cordero, B. M. Ross, A. J. Ricco and L. P. Lee, Stand-alone self-powered integrated microfluidic blood analysis system (SIMBAS), *Lab Chip*, 2011, **11**, 845–850.

31 S. Bakhtiaridoost, H. Habibiyan and H. Ghafoorifard, A microfluidic device to separate high-quality plasma from undiluted whole blood sample using an enhanced gravitational sedimentation mechanism, *Anal. Chim. Acta*, 2023, **1239**, 340641.

32 S. Garcia-Rey, J. B. Nielsen, G. P. Nordin, A. T. Woolley, L. Basabe-Desmonts and F. Benito-Lopez, High-Resolution 3D Printing Fabrication of a Microfluidic Platform for Blood Plasma Separation, *Polymers*, 2022, **14**, 2537.

33 I. K. Dimov, G. Kijanka, Y. Park, J. Ducrée, T. Kang and L. P. Lee, Integrated microfluidic array plate (iMAP) for cellular and molecular analysis, *Lab Chip*, 2011, **11**, 2701–2710.

34 S. Bakhtiaridoost, H. Habibiyan and H. Ghafoorifard, A microfluidic device to separate high-quality plasma from undiluted whole blood sample using an enhanced gravitational sedimentation mechanism, *Anal. Chim. Acta*, 2023, **1239**, 340641.

35 P. J. Carreau, Rheological Equations from Molecular Network Theories, *Trans. Soc. Rheol.*, 1972, **16**, 99–127.

36 E. Lecarpentier, M. Bhatt, G. I. Bertin, B. Deloison, L. J. Salomon and P. Deloron, *et al.*, Computational Fluid Dynamic Simulations of Maternal Circulation: Wall Shear Stress in the Human Placenta and Its Biological Implications, *PLoS One*, 2016, **11**, e0147262.

37 A. V. Priezzhev, O. M. Ryaboshapka, N. N. Firsov, I. V. Sirko and M. V. Lomonosov, Aggregation and disaggregation of erythrocytes in whole blood: study by backscattering technique, *J. Biomed. Opt.*, 1999, **4**, 76–84.

38 H. S. Tan and W. R. Pfister, Pressure-sensitive adhesives for transdermal drug delivery systems, *Pharm. Sci. Technol. Today*, 1999, **2**, 60–69.

39 I. Benedek and M. F. Mikhail, Technology of pressure-sensitive adhesives and products, *Handbook of Pressure-Sensitive Adhesives and Products*, CRC press, Three Volume Set, 2019.

40 R. Dhurat and M. Sukesh, Principles and methods of preparation of platelet-rich plasma: A review and author's perspective, *J. Cutan. Aesthet. Surg.*, 2014, **7**, 189.

41 R. E. Marx, Platelet-Rich Plasma: Evidence to Support Its Use, *J. Oral Maxillofac. Surg.*, 2004, **62**, 489–496.

42 X. Xie, C. Zhang and R. S. Tuan, Biology of platelet-rich plasma and its clinical application in cartilage repair, *Arthritis Res. Ther.*, 2014, **16**, 1–15.

43 K. Ficek, T. Kamiński, E. Wach, J. Cholewiński and P. Cięszczyk, Application of platelet rich plasma in sports medicine, *J. Hum. Kinet.*, 2011, **30**, 85–97.

44 A. Azari and C. J. Rapuano, Autologous serum eye drops for the treatment of ocular surface disease, *Eye Contact Lens*, 2015, **41**, 133–140.

45 N. Puri, Platelet rich plasma in dermatology and aesthetic medicine, *Our Dermatol Online.*, 2015, **6**, 207–211.

46 A. D. K. Le, L. Enweze, M. R. DeBau and J. L. Dragoo, Current clinical recommendations for use of platelet-rich plasma, *Curr. Rev. Musculoskelet. Med.*, 2018, **11**, 624–634.

47 J. Mercader Ruiz, M. Beitia, D. Delgado and P. Sanchez, Method based on ultrafiltration to obtain a plasma rich in platelet and plasma growth factors, *J. Clin. Med.*, 2023, **12**, 5941.

48 J. Mercader Ruiz, M. Beitia, D. Delgado, P. Sánchez, M. Begoña Sánchez and J. Oraa, *et al.*, Method to obtain a plasma rich in platelet-and plasma-growth factors based on water evaporation, *PLoS One*, 2024, **19**, e0297001.

49 I. A. Hagberg and T. Lyberg, Blood platelet activation evaluated by flow cytometry: optimised methods for clinical studies, *Platelets*, 2000, **11**, 137–150.

50 E. L. Welch, M. G. Crooks and S. P. Hart, Agreement between blood draw techniques for assessing platelet activation by flow cytometry, *Platelets*, 2019, **30**, 530–534.

51 H. P. Yaw, S. Van Den Helm, M. Linden, P. Monagle and V. Ignjatovic, Whole blood flow cytometry protocol for the assessment of platelet phenotype, function, and cellular interactions, *Platelets*, 2021, **32**, 786–793.

52 P. Wellings, Mechanisms of platelet capture under very high shear, *Cardiovasc. Eng. Technol.*, 2012, **3**, 161–170.

53 M. Panteleev, N. Korin, K. Reesink and D. L. Bark, Wall shear rates in human and mouse arteries: Standardization of hemodynamics for in vitro blood flow assays: Communication from the ISTH SSC, *J. Thromb. Haemostasis*, 2021, **19**, 588–595.

54 Y. Alvarez-Braña, J. Etxebarria-Elezgarai, L. Ruiz de Larrinaga-Vicente, F. Benito-Lopez and L. Basabe-Desmonts, Modular micropumps fabricated by 3D printed technologies for polymeric microfluidic device applications, *Sens. Actuators, B*, 2021, **342**, 129991.

55 P. E. Guevara-Pantoja, R. Jiménez-Valdés, J. L. García-Cordero and G. A. Caballero-Robledo, Pressure-actuated monolithic acrylic microfluidic valves and pumps, *Lab Chip*, 2018, **18**, 662–669.

56 J. J. Davis, M. Padalino, A. S. Kaplitz, G. Murray, S. W. Foster and J. Maturano, *et al.*, Utility of low-cost, miniaturized peristaltic and Venturi pumps in droplet microfluidics, *Anal. Chim. Acta*, 2021, **1151**, 338230.

57 T. Walker, Open Syringe Pump, **https://github.com/manimino/OpenSyringePump**, 2014.